Mon. Not. R. Astron. Soc. **397,** 548–557 (2009) doi:10.1111/j.1365-2966.2009.14968.x

H I content and star formation in the interacting galaxy Arp86

Chandreyee Sengupta,[1⋆] K. S. Dwarakanath[2⋆] and D. J. Saikia[1⋆]

[1]*National Centre for Radio Astrophysics, Tata Institute of Fundamental Research, Pune 411 007, India*
[2]*Raman Research Institute, Bangalore 560 080, India*

Accepted 2009 April 23. Received 2009 March 31; in original form 2009 January 12

ABSTRACT

We present the results of Giant Metrewave Radio Telescope (GMRT) observations of the interacting system Arp86 in both neutral atomic hydrogen, H I, and in radio continuum at 240 606 and 1394 MHz. In addition to H I emission from the two dominant galaxies, NGC 7752 and NGC 7753, these observations show a complex distribution of H I tails and bridges due to tidal interactions. The regions of highest column density appear related to the recent sites of intense star formation. H I column densities $\sim$1–1.5 $\times$ 10^{21} cm^{-2} have been detected in the tidal bridge which is bright in *Spitzer* image as well. We also detect H I emission from the galaxy 2MASX J23470758+2926531, which is shown to be a part of this system. We discuss the possibility that this could be a tidal dwarf galaxy. The radio continuum observations show evidence of a non-thermal bridge between NGC 7752 and NGC 7753, and a radio source in the nuclear region of NGC 7753 consistent with it having a low-ionization nuclear emission region nucleus.

Key words: galaxies: dwarf – galaxies: interactions – galaxies: spiral – radio continuum: galaxies – radio lines: galaxies.

1 INTRODUCTION

Galaxy interactions and mergers have been known to affect galaxy evolution in various ways and one such aspect is star formation in a galaxy. Since the early seventies, several theoretical and observational studies have been conducted to understand how star formation in a galaxy is altered or affected by collisions and mergers (Larson & Tinsley 1978; Biermann, Clarke & Fricke 1979; Woods & Geller 2007; Overzier et al. 2008). Several such studies have shown that prolonged enhancement of star formation is the cause of much of the infrared emission in major mergers (Sanders et al. 1986; Mihos & Hernquist 1994; Lin et al. 2007). Minor mergers or tidal interactions, which are common in moderate density environments like galaxy groups, also seem to affect the star formation rates (SFRs) and morphologies of galaxies. Many of these systems have been detected to have tidal bridges, tails and debris containing large amounts of H I with blue optical counterparts. However, it was not always clear whether the blue colour of these optical counterparts were due to the star-forming disc material pulled out in the interaction or due to in situ star formation in the tidal debris. The advent of ultraviolet (UV) and mid-infrared (MIR) telescopes like *Galaxy Evolution Explorer* (*GALEX*) and *Spitzer* have revealed bright recent star-forming clumps in the tidal debris (Hibbard et al. 2005; Neff et al. 2005; Smith et al. 2007). H I observations of such systems are important as these give us an estimate of the gas densities necessary to trigger star formation. Recent observations show evidence of star formation in remote sites away from the main disc, like tidal bridges and debris. The Magellanic bridge has been observed to host star formation in regions with N(H I) $\sim$$10^{20}$–$10^{21}$ cm^{-2} (Muller, Staveley-Smith & Zealey 2004; Harris 2007). The Arp's loop in M81−M82 system is undergoing recent star formation (de Mello et al. 2008). H II regions have been discovered in several systems, embedded in the tidal features (Ryan-Weber et al. 2004). Studying in situ star formation in tidal debris is of importance as this can also enrich the intergalactic medium (IGM) in addition to the galactic wind scenario (Ryan-Weber et al. 2004). Ryan-Weber et al. (2004) estimate that SFR as low as 1.5 $\times$ 10^{-3} M$_\odot$ yr^{-1} maintained for 1 Gyr can pollute the IGM with a metallicity $\sim$1 $\times$ 10^{-3} solar. This value compares well with the 'metallicity floor' $\sim$1.4 $\times$ 10^{-3} solar in the damped Lyman alpha (DLA) gas, observed over a redshift range of 0.5–5 (Prochaska 2003).

In order to study the H I gas properties such as the morphology, kinematics and column density distributions, and their correlation with the star forming zones, especially in the tidal bridges, tails and debris, we have presently chosen the remarkable but rather less studied interacting system Arp86. It is an archetypal example of interacting galaxies consisting of a grand-design barred spiral galaxy, NGC 7753, with a small companion, NGC 7752, towards the end of one of the spiral arms, much like the extensively studied M51 system. NGC 7753 has been classified as SAB(rs)bc in the NASA Extragalactic Data base (NED) and as SB(r)bc by Franco-Balderas et al. (2003), while NGC 7752 is classified as I0 by NED and as Irr

⋆E-mail: sengupta@ncra.tifr.res.in (CS); dwaraka@rri.res.in (KSD); djs@ncra.tifr.res.in (DJS)

Table 1. Some of the optical properties of Arp86.

	NGC 7753	NGC 7752
Major diameter[a]	3.3′	0.8′
Minor diameter[a]	2.1′	0.5′
Classification[a]	SAB(rs)bc	I0
Radial velocity[b]	5160 km s^{-1}	4940 km s^{-1}
Distance	68 Mpc	68 Mpc
K band mag[c] (absolute)	−25.5	−22.9
B band mag[c] (absolute)	−22.1	−19.7

[a]Nasa Extragalactic Data base.
[b]Marcelin et al. (1987).
[c]Apparent magnitude values from Nasa Extragalactic Data base.

galaxy by Nilson (1973). The optical diameter of NGC 7753 is 3.3 arcmin and that of NGC 7752 is 0.8 arcmin. Marcelin et al. (1987) have determined the heliocentric velocities of NGC 7753 and NGC 7752 to be 5160 and 4940 km s^{-1}, respectively, while the values listed in NED are 5168 and 5072 km s^{-1}, respectively. The distance to the system, using their average optical velocity and a Hubble constant of 75 km s^{-1} Mpc^{-1} is 68 Mpc (1 arcsec ∼0.33 kpc). Keel et al. (1985) note that in their sample of spiral galaxies, NGC 7753 is unusual in the small extent of the nuclear emission which appears unresolved. They classify NGC 7753 as a low-ionization nuclear emission region (LINER), while the brightest H II complex which contains many Hα knots occurs towards NGC 7752. Smith et al. (2007) present *Spitzer* MIR images of this system which is a part of their sample of interacting systems to study interaction-induced star formation. The *Spitzer* MIR observations show the presence of active star-forming regions in the spiral arms of NGC 7753, extending all the way to NGC 7752, in the form of a tidal bridge. Optical images also show the tidal bridge connecting the two galaxies, with bright regions of star formation in the bridge (Laurikainen, Salo & Aparicio 1993). Some of the optical properties of Arp86 are summarized in Table 1.

In order to investigate the correlation of gas properties and star formation in interacting systems, we observed this interesting system with the Giant Metrewave Radio Telescope (GMRT) in both H I and radio continuum at 240 and 606 MHz. The observations are described in Section 2, the observational results are presented in Section 3, while the results are discussed in Section 4. The main results are summarized in Section 5.

2 OBSERVATIONS

Arp86 was observed for 9 h in H I 21-cm line and for 3 h each at 606 and 240 MHz, in cycle 14 of GMRT observations. The GMRT is an interferometric array of 30 antennae, each of 45-m diameter, spread over a maximum baseline of 25 km. At frequencies of ∼1420 MHz, the system temperature and gain (K and KJy^{-1}) of the instrument are 76 and 0.22, respectively. System temperatures for 610 and 235 MHz are 102 and 237 K, and gains for these two frequencies are 0.32 and 0.33, respectively. The full width at half maximum of the primary beam of GMRT antennae is ∼24 arcmin at 1420 MHz, 43 arcmin at 610 MHz and 114 arcmin at 235 MHz. The baseband bandwidth used was 8 MHz for the 21 cm H I line observations (velocity resolution ∼13.7 km s^{-1}), 16 MHz for the 610 observations and 6 MHz for the 235 MHz observations. The observing log and the observational details are summarized in Table 2, which is self-explanatory. The pointing centre for all the observations was $23^{h}47^{m}01\overset{s}{.}61 + 29^{\circ}28'17\overset{''}{.}0$ in J2000 co-ordinates. The observations were done in the standard way with the phase calibrator observed before and after each scan on the source. The primary flux density and bandpass calibrator was 3C286 and 3C48 with an estimated flux density in the standard Baars flux density scale (Baars et al. 1977).

Data obtained with the GMRT were reduced using Astronomical Image Processing System (AIPS). Bad data due to dead antennae and those with significantly lower gain than others, and radio frequency interference (RFI) were flagged and the data were calibrated for amplitude and phase using the primary and secondary calibrators. The calibrated data were used to make both the H I line images and the 20-cm radio continuum images by averaging the line-free channels and self-calibrating. For the H I line images, the calibrated data were continuum subtracted using the AIPS tasks UVSUB and UVLIN. The task IMAGR was then used to get the final three-dimensional deconvolved H I data cubes. From these cubes, the total H I images and the H I velocity fields were extracted using the AIPS task MOMNT. While reducing the data at 240 and 606 MHz, a similar procedure as described above was followed. To avoid bandwidth smearing, the available baseband bandwidth was divided into smaller parts and used as input to the imaging task IMAGR. Multiple facets were used to cover the primary beam at both the lower frequencies. For both the frequencies, the field was divided into 31 facets and imaged. To bring out the structures on different levels in both H I and radio continuum, we produced images of different resolutions by tapering the data to different UV limits.

3 OBSERVATIONAL RESULTS

3.1 H I morphology

Fig. 1 presents the total H I column density map of the system with our lowest resolution of 40 arcsec, overlaid on Digitized Sky Survey (DSS) optical map and the integrated spectrum from the same data cube. A synthesized beam of this size samples the system with a spatial resolution of ∼13 kpc. The galaxy to the north-east is NGC 7753 and that to the south-west is NGC C7752. The total H I map reveals a very disturbed morphology, the presence of a tidal bridge between the two galaxies and H I in the form of tidal tails and debris around the system. The disc of NGC 7753 is rich in H I, though the centre shows depletion in the H I column density, possibly due to ongoing intense star formation. The bulk of the gas follows an arc like structure starting from the north-western edge of the disc of NGC 7753, following the optical bridge to the companion galaxy NGC 7752. Apart from these, there are two prominent spiral-arm-like features, one which points initially towards the north-east and then turns towards the west, while the other one is south of NGC 7752 and points towards the east. In neither of these two extensive H I features, any optical or MIR counterparts are seen. As we will refer to the observations and model of Laurikainen et al. (1993) and Salo & Laurikainen (1993), henceforth we will refer to the southern extension of H I from NGC 7753 as the H I bridge and the northern extension of H I as the tail, a nomenclature used in Laurikainen et al. (1993). We refer to the feature towards the south of NGC 7752, which was not seen in earlier observations, as the 'south-eastern extension'. Embedded in the tidal debris to the east, we detect a small galaxy, listed as '2MASX J23470758+2926531' in NED, which did not have any previous spectroscopic data. Our observations find this galaxy to be a part of this system.

From the spectrum shown in Fig. 1 which has a velocity resolution of 13.7 km s^{-1}, we estimate an integrated flux density of 18.7 Jy km s^{-1} which is smaller than the value of 22.7 Jy km s^{-1}

Table 2. GMRT observations.

Frequency	Observation date	Phase calibrator	Phase calibrator flux density (Jy)	τ (h)	Bandwidth (MHz)	rms (per channel for 21-cm line) (mJy beam^{-1})	Beam size (arcsec × arcsec)
21-cm line	2008 May 01	J0029 + 349	2.0	9	8	0.6	11 × 11
						0.8	25 × 25
						1.0	40 × 40
1394 MHz	2008 May 01	J0029 + 349	2.0	–	–	0.4	16 × 16
606 MHz	2008 May 23	J0137 + 331	29.5	3	16	0.6	16 × 16
240 MHz	2008 May 23	J0137 + 331	51.8	3	6	1.5	16 × 16

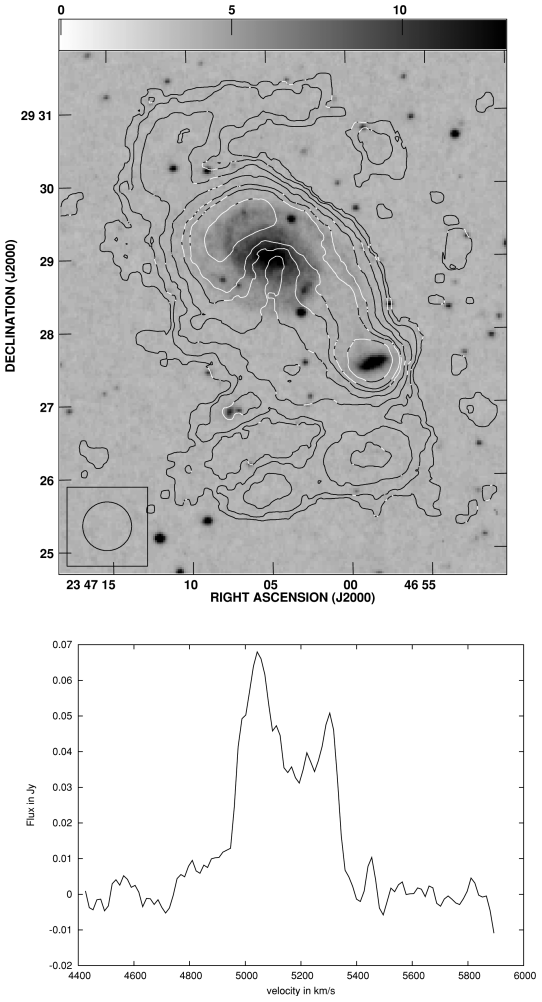

Figure 1. Upper pannel: H I column density map of Arp86 with an angular resolution of 40 arcsec overlaid on an optical DSS map. The H I column density contours are $1.4 \times 10^{19} \times (3, 7, 15, 25, 40, 50, 70)\,\mathrm{cm}^{-2}$. Lower pannel: the GMRT H I spectrum of Arp86 obtained with an angular resolution of 40 arcsec.

estimated from single-dish observations (Huchtmeier & Richter 1989), suggesting that there could be more diffuse emission which is not visible in our image. We detect $2.1 \times 10^{10}\,\mathrm{M}_{\odot}$ of H I mass from the Arp86 system using our lowest-resolution image.

The channel maps and the first-moment image, which represents the intensity-weighted velocity field, with an angular resolution of 40 arcsec are shown in Figs 2 and 3,, respectively. The H I channel maps show a clear connection between NGC 7753 and NGC 7752 in velocity space. The spiral feature in the north of NGC 7753, referred to as the tail, is visible at velocities ranging from ∼5330 to 5070 km s^{-1}, with the highest velocities occurring towards the north-eastern end of NGC 7753. The gas in the disc of this galaxy shows signs of rotation, with the south-eastern side approaching us. The gas in the bridge connecting the two galaxies is approaching us, with the velocities in NGC 7752 extending up to ∼4800 km s^{-1}. In the eastern side, gas is seen towards 2MASX J23470758+2926531 over a range of velocities extending from 4963 to 5181 km s^{-1}. The velocity field of the south-eastern extension ranges from ∼4936 km s^{-1} south of NGC 7752 to ∼5150 km s^{-1}. This is close to the velocity seen in the galaxy 2MASX J23470758+2926531. It is interesting to note that there appears to be weak emission seen in the low-resolution H I image (Fig. 1) connecting the edge of the south-eastern feature to the 2MASX galaxy. The nature of this galaxy is discussed later in the paper.

The H I column density image superposed on the optical DSS image and the velocity dispersion with an angular resolution of 25 arcsec, which corresponds to about 8 kpc, are shown in Fig. 4. The regions with high velocity dispersions of >50 km s^{-1} are seen towards NGC 7752, the galaxy 2MASX J23470758+2926531 and towards the eastern end of the 'south-eastern extension'. There also appears to be a region of high velocity dispersion between NGC 7752 and 2MASX J23470758+2926531, but this could be due to low signal-to-noise ratio and needs confirmation. The rest of the emission has velocity dispersions less than this value. It may be relevant to note here that in this image the 'south-eastern' extension appears disjointed from the Arp86 system.

To explore possible correlations of star-forming regions of the system with H I column density, we have made an H I column density image with a higher angular resolution of 11 arcsec which corresponds to ∼3.6 kpc. The higher resolution helps to minimize dilution of the estimate of the column density from more diffuse emission. This high-resolution image is shown superimposed on the 24 μm *Spitzer* MIR in Fig. 5. The star-forming regions in the system are seen as the dark patches in the grey-scale MIR image. The H I image shows clumps and knots of emission with peak column densities in the range of 1–4 × $10^{21}\,\mathrm{cm}^{-2}$, and absence of emission towards the centre of NGC 7753. The regions of high star formation towards the eastern and northern edges of NGC 7753 and then following the bridge between the two galaxies and also the emission from NGC 7752 appear to correlate with the regions of highest column density. There is also a region of star formation towards the south-western edge of NGC 7753, where high-column density H I gas is seen.

3.2 Radio continuum

The radio continuum images at 240 606 and 1394 MHz of NGC 7752 and NGC 7753 with angular resolutions of 45 and

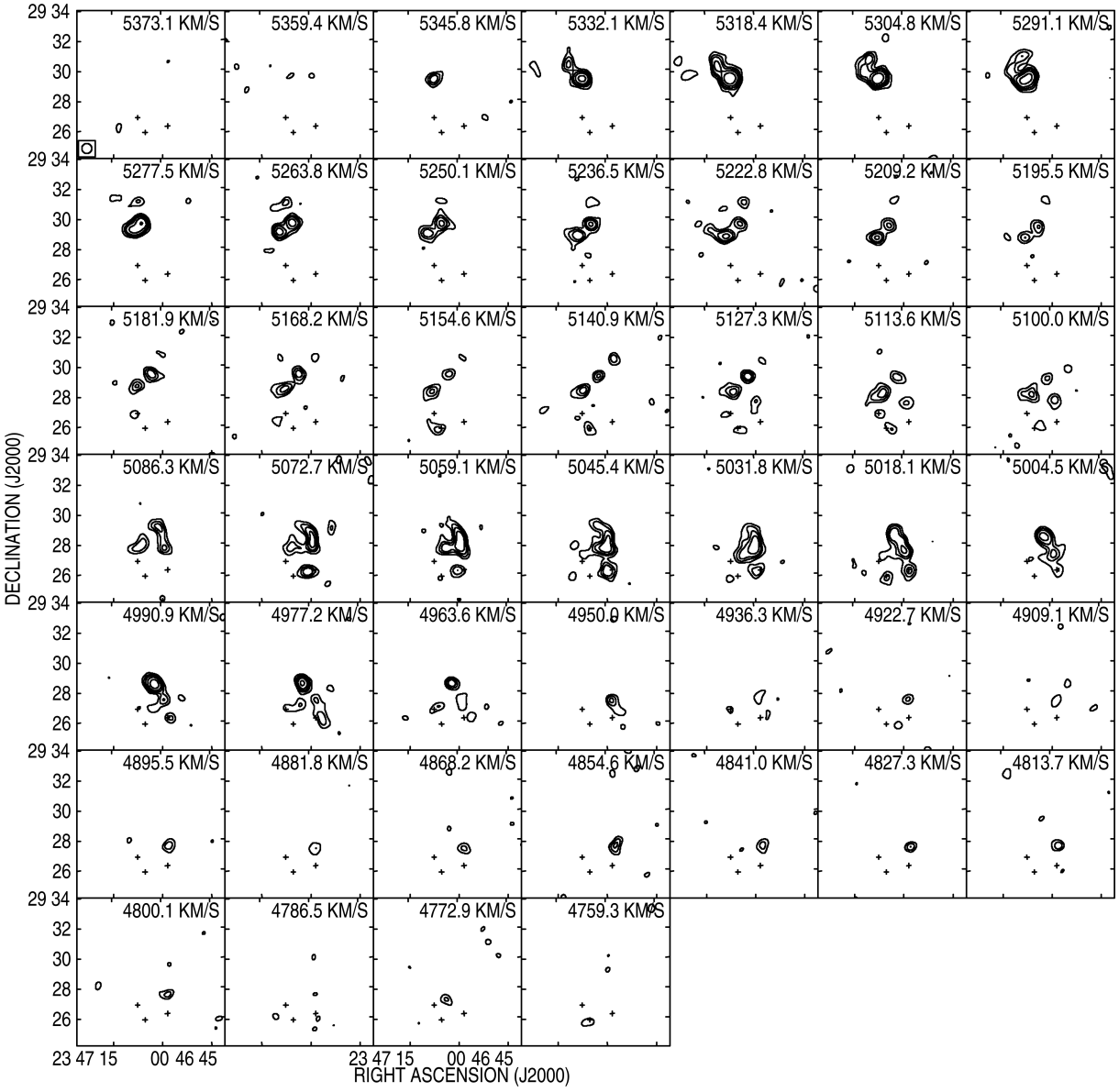

Figure 2. The channel images of Arp86 with an angular resolution of 40 arcsec. The contour levels are 1 mJy beam^{-1} × (3, 5, 7, 10, 15). The first plus sign (from left) denotes position of 2MASX J23470758 + 2926531, the next two '+' signs denote the two H I peaks in the south-eastern H I extension. The signs help to understand the location of H I in this region.

16 arcsec, which correspond to ∼15 and 5 kpc, respectively, are presented in Figs 6 and 7, respectively. Amongst the low-resolution images, the 606 MHz one which has an rms noise of 0.64 mJy beam^{-1} shows clear evidence of a radio continuum bridge connecting the galaxies NGC 7752 and NGC 7753. Although there may be some evidence of this bridge at 240 MHz, it is not seen clearly at 1394 MHz (Fig. 6). The higher-resolution images of the system presented in Fig. 7 have all been smoothed to the resolution obtained at 240 MHz. The small galaxy, 2MASX J23470758+2926531, was not detected in radio continuum, in any of these three bands.

Radio continuum emission from NGC 7752 seems to be star formation dominated and shows it to be well resolved at the highest resolution (7 × 3 arcsec^2) image. The total flux densities obtained from the images at different frequencies are summarized in Table 3.

The low-resolution images of NGC 7753 show that it is dominated largely by diffuse disc emission, although its structure appears somewhat different at the different frequencies, which may be at least partly due to different mixtures of thermal and non-thermal emission. The total flux densities estimated from the low-resolution images over similar areas are presented in Table 3. The typical uncertainties in the flux density estimates at 1394 and 606 MHz are ∼5 per cent and at 240 MHz ∼18 per cent. However, given the quality of the image and the relatively lower surface brightness of the diffuse emission from NGC 7753, the uncertainty in its flux density could be somewhat higher. At 240 MHz, the disc emission is seen to have two peaks, both of which correlate with the star-forming regions in the disc. The set of high-resolution maps also show fragmented emission, largely coinciding with the star-forming regions. These observations also reveal the presence of a weak compact central source in NGC 7753, which has not been noted earlier. The position of this compact source whose peak at $23^{\rm h}47^{\rm m}04\overset{\rm s}{.}40 + 29^\circ29'01\overset{''}{.}2$ is coincident within the errors with the

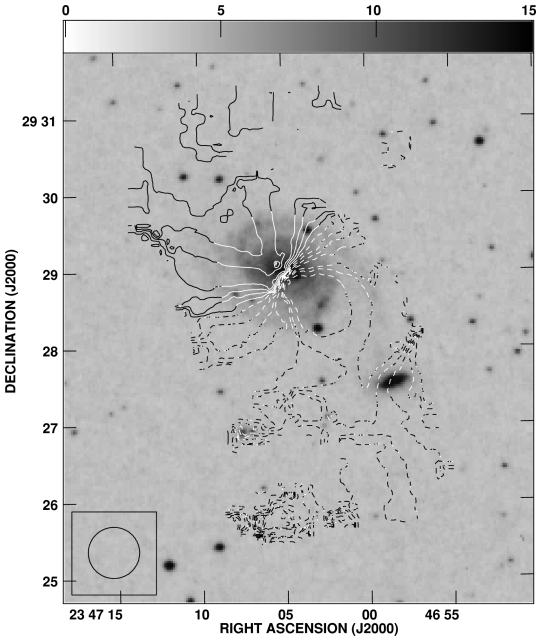

Figure 3. H I velocity field of Arp86 with an angular resolution of 40 arcsec, overlaid on an optical DSS image. Velocity levels: (−300, −250, −200, −160, −130, −110, −70, −50, −30, −10, 10, 30, 50, 70, 110, 130, 140) km s^{-1} relative to the central velocity of 5168 km s^{-1}.

optical centre of the galaxy located at $23^{h}47^{m}04\overset{s}{.}8 + 29^{\circ}29'00\overset{''}{.}4$ (NED). The flux densities of the central component estimated from the images in Fig. 7 are listed in Table 3. The flux densities of this feature are similar even when one considers the highest resolution images at 606 and 1394 MHz. The spectra obtained from these measurements are presented in Fig. 8 and are discussed in section 4.6.

4 DISCUSSION

Arp86 is similar to an M51 type system, with a grand-design main galaxy interacting with a small galaxy at the tip of one of its arms. Arp86 has been studied in detail and modelled to understand the nature of interaction induced star formation in the system (Laurikainen et al. 1993; Salo & Laurikainen 1993). Recent *Spitzer* observations in the MIR provide quite a detailed picture of the tidally induced star formation sites in the system and reveal a tidal bridge with ongoing star formation (Smith et al. 2007). To search for interaction-enhanced star formation in the MIR, instead of comparing luminosities, which measure the absolute SFR, the authors suggest that it is better to compare the *Spitzer* colours, which measure mass-normalized SFRs. The bands in which these observations were carried out were 3.6, 4.5, 5.8, 8.0 and 24 μm. The 4.5–5.8, 3.6–8.0, 8.0–24 and 3.6–24 colours are all measures of the mass-normalized SFR, with a redder colour indicating a higher normalized SFR. The 3.6- and 4.5-μm bands are dominated by the older stellar population, while the other bands have significant contributions from interstellar dust heated by young stars. For the set of M51-like systems in this sample of Arp galaxies, of which Arp86 is a member, the authors note redder 8.0–24, 3.6–24 and 5.8–24 colours and a general enhancement of SFR, especially enhancements that are localized in some regions of the system. This is in agreement with the results of Laurikainen et al. (1993), who found bluer optical colours in the central regions of 9 out of 13 M51-like galaxies they studied including a detailed study of Arp86.

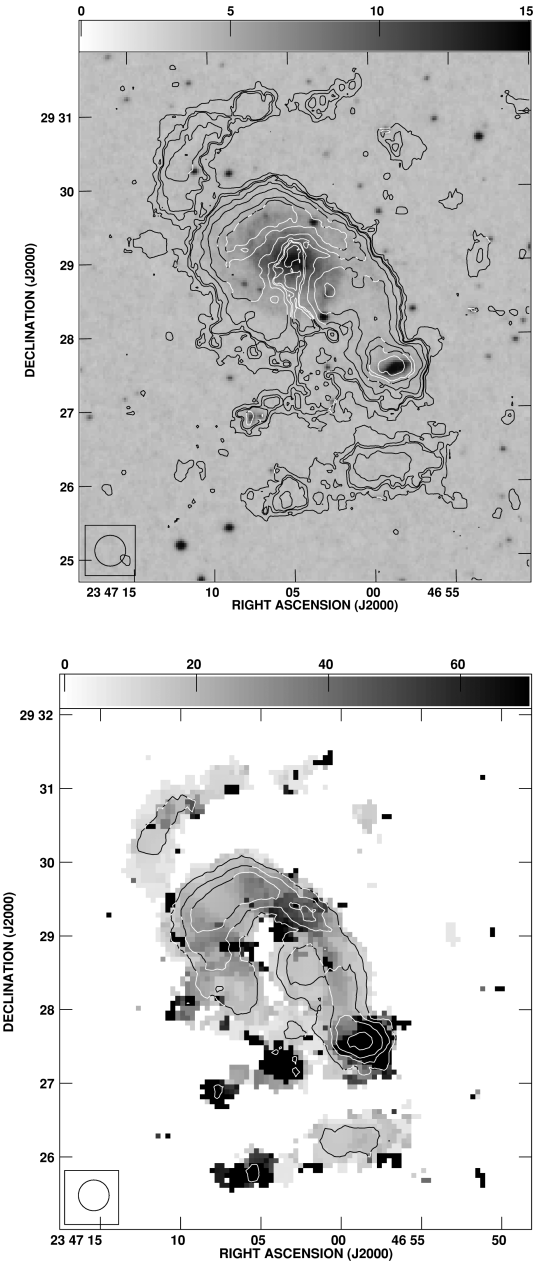

Figure 4. Upper panel: H I column density map of Arp86 with an angular resolution of 25 arcsec overlaid on an optical DSS map. The H I column density contours are $2.5 \times 10^{19} \times (3, 7, 9, 15, 25, 40, 50, 70)$ cm^{-2}. Lower panel: H I contours overlaid on grey-scale H I velocity dispersion map with an angular resolution of 25 arcsec. The velocity dispersion range is from 0 to 70 km s^{-1}. H I column density contours are $1.8 \times 10^{19} \times (20, 40, 60, 100)$ cm^{-2}.

4.1 H I morphology

H I observations of interacting systems are very useful to probe a number of aspects. They enable us to probe the distribution of gas due to the interactions and constrain theoretical models, probe regions of star formation which may be induced by the interactions and examine correlations of star formation sites with H I column density, and explore the formation and properties of tidal dwarf galaxies.

The H I features in Arp86 resemble those of M51 in many ways, which have been modelled as being due to tidal interactions between

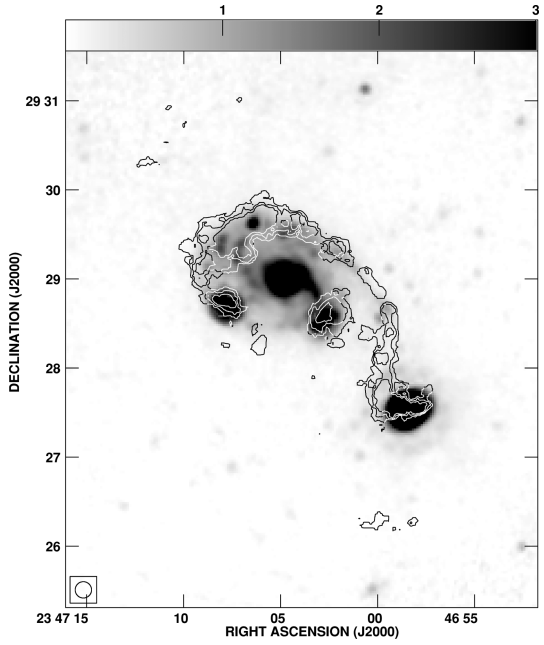

Figure 5. The H I column density image of Arp86 with an angular resolution of 11 arcsec overlaid on the *Spitzer* 24-μm image. The H I column density contours are $1 \times 10^{20} \times (10, 15, 20)\,\mathrm{cm}^{-2}$.

the two galaxies (Howard & Byrd 1990). As discussed earlier, the low-resolution H I images of Arp86 reveal large (∼4 arcmin) gaseous tidal arms and debris, towards both the north and south of the system. An H I bridge connects NGC 7753 to its smaller mass companion NGC 7752. H I debris seen beyond that, towards the south, may either be an extension of a tidal arm or may be material pulled out from the system and dumped in the IGM. In the channel maps, the southern debris seems to have a continuity from 4936 to 5154 km s^{-1}. A detailed high-resolution Hα velocity field study of Arp86 (Marcelin et al. 1987) found a steep velocity gradient in NGC 7752 and an anomalous velocity distribution between 4920 and 5060 km s^{-1} towards its north-eastern region. More importantly, the north-eastern edge of NGC 7752 and the bridge end, where it joins NGC 7752, share similar radial velocities ∼5060 km s^{-1}. The authors suggested this could be a signature of a tidal tail/bridge about to be torn from NGC 7752. Our H I map reveals tidal debris at this position, matching the velocities suggested by Marcelin et al. (1987). Though we lack the necessary resolution to study the velocity field of NGC 7752 in detail, our H I channel maps show the southern debris to start at ∼4936 km s^{-1}, close to the velocity of 4920 km s^{-1} suggested by Marcelin et al. (1987). In the lowest resolution H I map (40 arcsec), the southern debris seems to be loosely connected to the main system of Arp86. However, in the 25-arcsec map, the debris looks detached from the system, quite as suggested in Marcelin et al. (1987). However, even though it appears detached, the debris has a continuity in the velocity space till ∼5150 km s^{-1}.

Towards the north of Arp86, an H I tidal tail of ∼4 arcmin in length, which corresponds to ∼80 kpc is seen. It initially points towards the north-east, then curves towards west and later runs almost parallel to the tidal bridge between NGC 7753 and NGC 7752. This feature is continuous in velocity space between 5330 and 5070 km s^{-1}. A similar feature was noted in the H I images of the M51 system by Rots et al. (1990). A long H I tail without any optical counterpart was seen to be connected loosely to the disc of NGC 5194. A detailed simulation involving three components, stars, gas clouds and dark halo and taking into account collision of the gas clouds could reproduce most of the H I features of M51 successfully, but not the extended H I tail (Howard & Byrd 1990). The H I tail was proposed to be a remnant of the previous passage of the companion. The ratio of the masses of the companion NGC 5195 to the main galaxy NGC 5194 in case of the M51 system needed to be roughly 0.1 for the simulation to be able to reproduce the observational features (Howard & Byrd 1990). From the Hα rotation curves, the masses of NGC 7753 and NGC 7752 were estimated to be 1.3×10^{11} and $1.8 \times 10^{10}\,\mathrm{M}_{\odot}$, respectively (Marcelin et al. 1987). This makes the mass ratio of the companion to the main galaxy ∼0.1, a value similar to that of the M51 system (Howard & Byrd 1990). The results from the simulations and rotation curve analysis of Salo & Laurikainen (1993) suggests M51-like interaction in the Arp86 system involving multiple passages of the companion around the main galaxy. Perturbation by a companion at closed orbit involving multiple passages may lead the main disc to exhibit open spiral structures (Salo & Laurikainen 1993). M51 is an example of this, and our observations show this for Arp86 as well. Simulation results of Salo & Laurikainen (1993) indicate a spiral arm towards the north of Arp86, but our H I observations show a much more extended feature than expected in Salo & Laurikainen (1993). However, taking

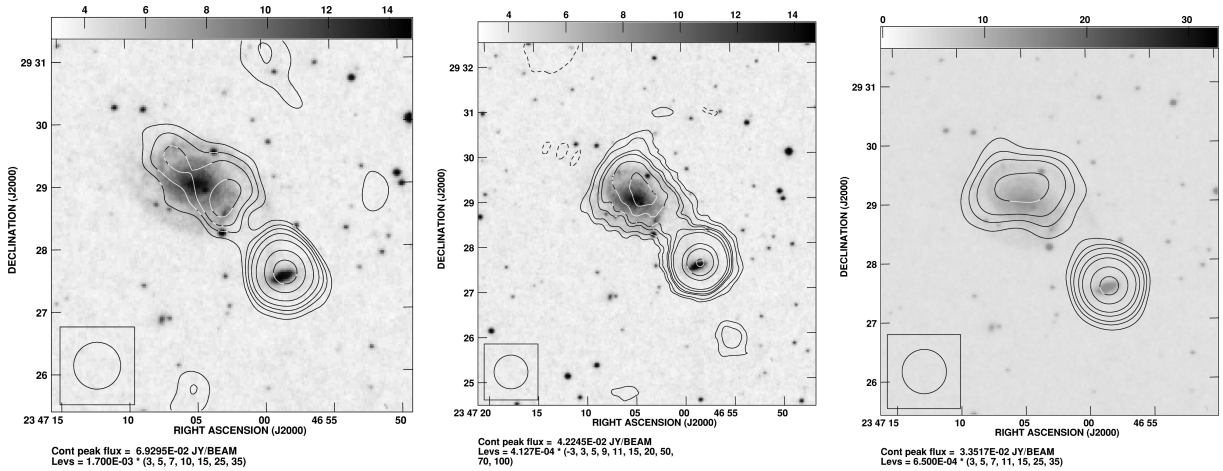

Figure 6. The radio continuum images of Arp86 with an angular resolution of 45 arcsec at 240 (left-hand panel), 606 (middle panel) and 1394 (right-hand panel) MHz.

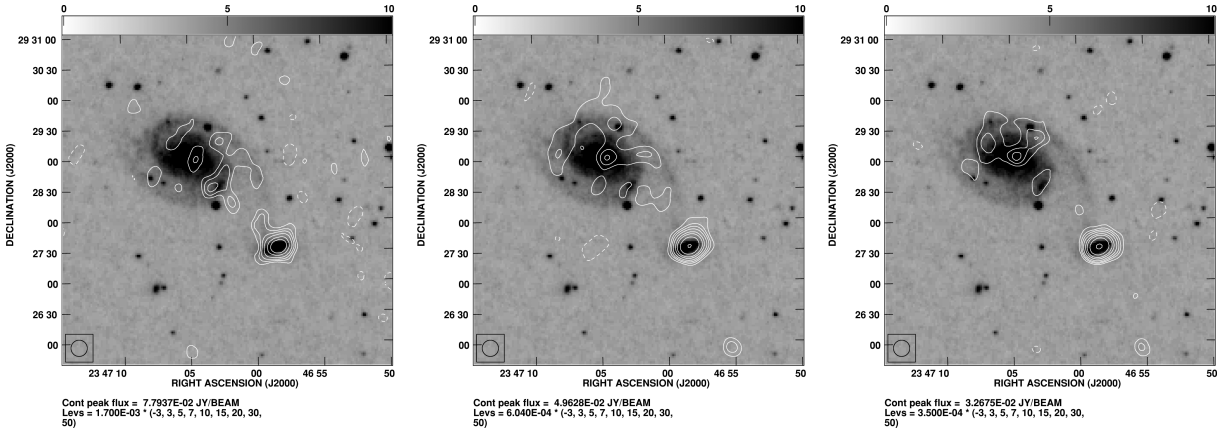

Figure 7. The radio continuum images of Arp86 with an angular resolution of 16 arcsec at 240 (left-hand panel), 606 (middle panel) and 1394 (right-hand panel) MHz.

Table 3. Estimates of radio continuum integrated flux densities.

Frequency (MHz)	Beam size ($''$)	NGC 7752 (mJy)	NGC 7753 (mJy)	NGC 7753 (core) (mJy)
1393.8	45	26	21	–
	16	25	–	2.6
606.5	45	46	26	–
	16	45	–	4.5
240.0	45	69	∼50	–
	16	76	–	9.1

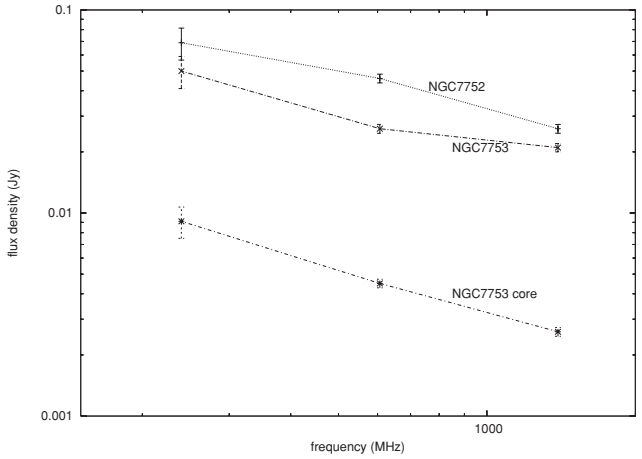

Figure 8. Continuum spectra from the Arp86 system.

the example of M51 (Howard & Byrd 1990; Rots et al. 1990) and taking into consideration that the interactions of M51 and Arp86 are of similar nature, the long northern tidal tail of Arp86 can be a remnant from the past passage of the companion.

The velocity field of Arp86 has been studied in detail using Hα observations by Marcelin et al. (1987). Isovelocity contours reveal normal differential rotation in both the discs. However, signature of warping was found in the western side of NGC 7753, the position angle of the major axis was seen to bend towards NGC 7752. Even NGC 7752 was reported to appear warped towards its north-eastern edge, where isovelocity contours were found to be quite disturbed, following typical signs of interaction. Our H I observations of coarser resolution show that the velocity field exhibits regular disc rotation in NGC 7753, with the velocity reaching a maxima at ∼5340 km s^{-1} towards the north-east which is the receding side. These numbers are in agreement with the Hα velocity field observed by Marcelin et al. (1987). On the western side of the NGC 7753, the velocity field is disturbed and chaotic possibly due to the interactions.

4.2 Star formation in the tidal bridge and tail

The optical *BVRI* photometry (Laurikainen et al. 1993) and the *Spitzer* images (Smith et al. 2007) suggest that this system has undergone a recent enhancement of star formation, possibly induced by the interaction. Laurikainen et al. (1993) find the bridge to be bluer than the tail. Our high-resolution image of H I column density shows the emission to be an arc-like structure, with the highest column density gas towards the star-forming regions (Fig. 5). Laurikainen et al. (1993) identify two regions, one in the north and the other in the south of the disc of NGC 7753, as regions of high star formation. The *Spitzer* images (Smith et al. 2007) are consistent with the regions identified by Laurikainen et al. (1993). The H I column density in these regions are amongst the highest and the peaks range from ∼1–4 × 10^{21} cm^{-2}. The galaxy NGC 7752 and the small galaxy 2MASX J23470758+2926531, in the eastern side also appears bright in the *Spitzer* image, possibly due to star formation induced by the interaction.

Of all the *Spitzer* bands, the 24-μm band seems to be the best suited for tracing recent star formation. This band is dominated by emission from very small grains heated by the UV radiation field. Calzetti et al. (2005) find a tight correlation between Paα and 24-μm flux density, implying 24-μm flux density is well suited for tracing the current H II regions. The 8-μm flux density, which is commonly associated with the larger sized polycyclic aromatic hydrocarbons (PAHs), also correlates with the Paα flux density, but with some non-linearity. To trace SF regions, this band may not be the best as the large PAH molecules are often destroyed by the high-intensity ionizing radiation deep inside an H II region. Using the empirical formula from Calzetti et al. (2005) and the 24-μm flux densities from Smith et al. (2007), we derive the SFR in Arp86. Smith et al. (2007) provides the global 24-μm flux density from NGC 7753, NGC 7752 and the tidal bridge. Accordingly, the SFRs associated with NGC 7753, NGC 7752 and the tidal bridge are 9.0, 7.1 and 0.6 M$_\odot$ yr^{-1}, respectively.

4.3 Threshold H I column densities

Kennicutt (1989) showed that for a self-gravitating gas disc, there must be a threshold H I column density for star formation to set in. The range of this threshold density varies in the range 10^{20}–10^{21} cm^{-2} (Kennicutt 1989). For irregular galaxies, Skillman (1987) found this limit to be 10^{21} cm^{-2}, averaged over 500 pc within the discs. They also found that for giant H I regions to form, the gas density needs to be few times more than this threshold density and below this threshold star formation is actually suppressed in the observed galaxies. Recent observations over the last decade contain evidence of star formation happening in a varied range of densities. The H I bridge in the Magellanic Clouds, which has typical column densities $\sim 10^{20}$–10^{21} cm^{-2} is known to have star formation happening in it (Harris 2007). However, no intense star formation is seen to happen in the more diffuse Magellanic stream with $N(\mathrm{H\,I}) \leq 3$–5×10^{20} cm^{-2} (Bruns et al. 2005). In denser environments, Hibbard et al. (2005) reported intense star formation in the tidal bridges of the antennae. Maybhate et al. (2007) report of a critical H I column density value of $N(\mathrm{H\,I}) > 4 \times 10^{20}$ cm^{-2} over kiloparsec scale for superstar clusters to form. More recently, de Mello et al. (2008) reported star formation in the tidal bridge between M81 and M82, where $N(\mathrm{H\,I})$ is ~ 5–30×10^{20} cm^{-2}. All these observations more or less agree with the fact that high H I column density regions are associated with the high star formation zones in the discs of galaxies. The thresholds found in different studies could be different for two reasons. First, the scales over which the average H I column densities are quoted are not the same for all observations. Bigger areas can dilute the column densities and therefore the numbers quoted will reflect a lower threshold than the actual one. And second, the threshold density (Toomre 1964) may be a crucial parameter for forming stars, but it may not be the sole defining factor for star formation to set in (Kennicutt 1989).

Our observations of star formation happening in the Arp86 system is in general agreement with the above-mentioned observations. We do find that star-forming zones are associated with regions of high-density H I clouds in the discs of the two galaxies of Arp86. Even in the tidal bridge (SFR $\sim 0.6\,\mathrm{M}_\odot$ yr^{-1}), which is a region of $N(\mathrm{H\,I})$ ~ 1–1.5×10^{21} cm^{-2} averaged over scales of ~ 3 kpc, we note a positive correlation of the *Spitzer* bright regions to high H I column density regions.

4.4 H I velocity dispersion

NGC 7753 and NGC 7752 have inclination angles $i \sim 49^\circ$ and 75°, respectively. Fig. 4 shows the dispersion in NGC 7752 to be high (>60 km s^{-1}), possibly due to the inadequate resolution of the observations. In NGC 7753, the velocity dispersion ranges from 6 to 50 km s^{-1}.

The two regions of intense star formation identified by Laurikainen et al. (1993) have a dispersion ≤ 25 km s^{-1}. But some areas in the tidal bridge, where star formation is going on, have a higher value of dispersion ~ 50 km s^{-1}. Opinion, about whether dispersion should be high or low in the star-forming zones, is divided in literature. Though there are some suggestions that dispersion should be low for the gas to gravitationally collapse and form stars, observational evidences point towards a varied range of dispersion values in the star-forming zones. While some observations have shown high H I dispersion to correlate with regions of low or no star formation (Ryan-Weber et al. 2004), some have seen enhanced dispersion (~ 40 km s^{-1}) to correlate with H II regions (Irwin 1994). Also a simple correlation of dispersion and star-forming region should not be expected as it is difficult to identify the cause–effect relation between the two. In principle, high dispersion can lead to high star formation as the Jeans mass is proportional to the fourth power of dispersion (Elmegreen, Kaufman & Thomasson 1993) or it can be an effect of high star formation, if the cloud is randomized by the outflows of massive star formation activity (Irwin 1994). The situation in this system is also unclear. We find regions of low dispersion in the disc of NGC 7753, medium dispersion in the tidal bridge and high dispersion in NGC 7752 and the galaxy 2MASX J23470758+2926531, and all of these being star-forming regions. Also, we see high velocity dispersion of >60 km s^{-1} towards the eastern edge of the south-eastern feature, without any evidence of star formation.

4.5 2MASX J23470758+2926531: a tidal dwarf galaxy?

As discussed in Section 3, our observations show the galaxy 2MASX J23470758+2926531 to be a part of the Arp86 system. We estimate the stellar mass of this galaxy using its K-band magnitude and $K - J$ colours, listed in NED. The mass-to-light ratio of galaxies in the K-band (M/L_K) are related to the $K - J$ colours by the equation (Bell & de Jong 2001)

$$\log(M/L_K) = a_K + b_K \mathrm{colour}_{K-J}, \quad (1)$$

while the luminosity in the K-band, L_K is related to the absolute magnitude in the K-band (M_K) as (Worthey 1994)

$$L_K(\mathrm{L}_\odot) = \exp\left[0.921034\,(3.33 - M_K)\right]. \quad (2)$$

The estimated absolute K magnitude is -20.3 and the stellar mass of this galaxy is $2.9 \times 10^9\,\mathrm{M}_\odot$. The H I mass, estimated from the spectrum (Fig. 9) is $4.5 \times 10^8\,\mathrm{M}_\odot$. The spectrum suggests a weak double horn, consistent with rotation, although the spectrum could be affected by more extended tidal features near the galaxy. It is interesting to enquire whether this galaxy might be a tidal dwarf galaxy (TDG). TDGs are known to be comparable in luminosity to typical dwarfs, though metallicities can be higher in TDGs. They have characteristic blue colours as a result of active starburst, high velocity dispersion and can have high H I masses $\sim$ few times $10^8\,\mathrm{M}_\odot$ and stellar masses $\sim$ few times $10^9\,\mathrm{M}_\odot$ (Duc et al. 2000). Our TDG candidate is similar to the above stated galaxies in terms of stellar and H I mass, physical extent and high dispersion values (≥ 50 km s^{-1}). The galaxy is bright in the *Spitzer* and *GALEX* images, indicating recent star formation. The properties are consistent with that of a TDG. The dynamical mass of 2MASX

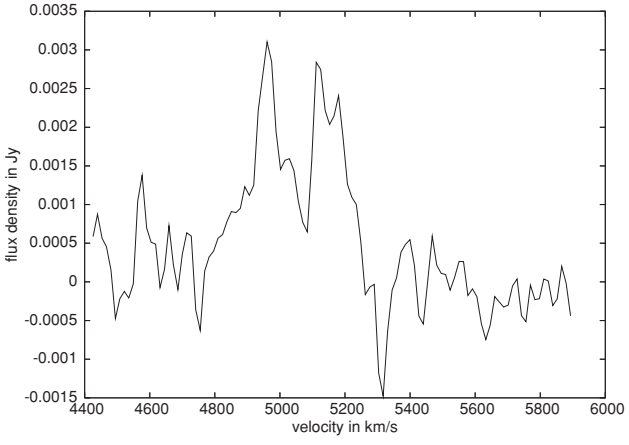

Figure 9. H I spectrum of 2MASX J23470758+2926531.

J23470758+2926531 has been estimated using the rotation velocity as observed in the H I spectrum and a radial extent ∼12.5 arcsec. This is half the beam width of our H I image (Fig. 4) and corresponds to ∼4 kpc. The mass thus derived is $1.4 \times 10^{10}\,M_{\odot}$. This makes the $M_{\rm dynamical}/L_{K\,\rm band}$ ratio to be 4.8. For TDG candidates, this number is expected to be small due to lack of dark matter. The median value for the mass-to-light ratios of the TDG candidates in Stephan's Quintet was found to be 7.0 (Amram et al. 2002). Judging by these arguments, it is likely that 2MASX J23470758 + 2926531 is a candidate TDG in Arp86 system. However, occurrence of TDGs in such unequal mass systems is very rare. Most of the known candidate TDGs have formed during roughly equal mass strong interactions which has brought out a large amount of gas out of the galaxies' discs, e.g. TDGs in Arp105 (Ferreiro, Pastoriza & Rickes 2008), NGC 3227/3226 (Mundell et al. 2004), Arp245 (Duc et al. 2000). Garland, formed in the interaction of NGC 3077/M81, is one of the few known TDG candidates to form in an encounter involving highly unequal mass galaxies (Karachentsev, Karachentseva & Boerngen 1985). Although we suggest this to be a TDG candidate from the available information, the possibility that this might be a small galaxy which has been part of the Arp86 group cannot be ruled out.

4.6 Radio continuum emission

As mentioned earlier, radio continuum emission has been detected from both NGC 7752 and NGC 7753, and from a bridge between the two galaxies, but no emission has been detected from the candidate TDG. The spectrum of radio emission from NGC 7752 shows some evidence of steepening towards higher frequencies. The spectral indices (SI) of NGC 7752 is ∼0.4 between 240 and 606 MHz and ∼0.7 between 606 and 1394 MHz. This is consistent with the finding of Hummel (1990) who estimates a median break frequency of approximately 700 MHz for a sample of spiral galaxies. A shallow low-frequency spectral index of ∼0.4 for the disc emission in NGC 7752 is on the lower side. In the sample of 27 spiral galaxies studied by (Hummel 1990), only three of his galaxies have a low-frequency (below ∼1 GHz) SI less than 0.4. Modelling the steepening of the spectrum in the sample of sources as being due to propagation and energy loss processes, the author equates the asymptotic low-frequency SI to the injection spectral index and finds the values to be in the range of 0.3–0.6 with a median value of $\sim 0.40 \pm 0.05$. Our low-frequency SI of NGC 7752 is consistent with this interpretation.

The SI of the extended emission in NGC 7753 is ∼0.7 between 240 and 606 MHz, similar to the low-frequency SIs of several of the galaxies studied by Hummel (1990). However, the radio emission from this galaxy shows evidence of flattening between 606 and 1394 MHz, with a SI of 0.25, which needs to be confirmed from higher-frequency observations. The 1400-MHz flux density from NRAO VLA Sky Survey (NVSS) is also consistent with this flattening of the higher frequency radio spectrum. This would suggest that thermal free–free emission could also play a significant role in determining the spectral shape. This is also suggested by the rather high SFR of $9.0\,M_{\odot}\,{\rm yr}^{-1}$ in this galaxy. It is relevant to note that the galaxies in the sample of Hummel (1990) which show evidence of flattening of the high-frequency spectrum are NGC 253, NGC 1569 and NGC 5236, all of which show evidence of a strong starburst.

The radio 1400-MHz and far-infrared (FIR) 60−μm luminosities of NGC 7752 are 22.1 and 10.3 (in log scale), respectively, while the corresponding values for NGC 7753 are 20.3 and 8.3, respectively. These values are consistent with the radio-FIR correlation (Yun, Reddy & Condon 2001). This is an expected result since none of these galaxies have prominent active galactic nuclei. The radio luminosities at 1400 MHz indicate a supernova rate of 0.10 and 0.08 for NGC 7752 and NGC 7753, respectively, using the formalism of Condon & Yin (1990). These numbers are consistent with the supernova rate estimates made using lower frequency flux densities as well. The supernova rates for NGC 7752 and NGC 7753 appear similar to estimates for other galaxies with different degrees of starburst activity. These estimates include ∼0.04–0.1 $\rm yr^{-1}$ for a small sample of galaxies including the archetypal starburst galaxy NGC 1808 (Collison et al. 1994), ∼0.1 $\rm yr^{-1}$ for M82 (Huang et al. 1994), ≤0.1–0.3 for NGC 253 (Ulvestad & Antonucci 1997), ∼0.1 $\rm yr^{-1}$ for the irregular starburst galaxy Mrk 325 (Condon & Yin 1990) and the starburst galaxy NGC 3448 of the Arp 205 system (Noreau & Kronberg 1987), ∼0.07 $\rm yr^{-1}$ for NGC 6951 (Saikia et al. 2002) and ∼0.14 $\rm yr^{-1}$ for the superwind galaxy NGC 1482 (Hota & Saikia 2005).

For both NGC 7752 and NGC 7753, we have estimated the minimum energy, equipartition magnetic field and spectral ages by integrating the spectrum between 10 MHz and 100 GHz, a filling factor of unity and an electron to proton energy density ratio of unity. For NGC 7753, whose high-frequency spectrum is likely to be affected by thermal emission, we have assumed a SI of 0.7 between 10 MHz and 100 GHz. The minimum energy and the equipartition magnetic fields for NGC 7752 are 8.1×10^{53} erg and 3.6 μG and for NGC 7753 are 5.9×10^{54} erg and 2.6 μG. The spectral ages of NGC 7752 and NGC 7753 for a break frequency of 600 MHz are $\sim 1.1 \times 10^{8}$ yr and 1.7×10^{8} yr, respectively.

The radio continuum emission also shows a bridge of emission between the two galaxies which is seen clearly in the 606-MHz image with a resolution of 45 arcsec. Although H I bridges have been seen in many interacting systems, radio continuum bridges are less common. This could be at least partly due to the absence of a systematic search for radio continuum bridges at low frequencies, where these bridges are expected to be more prominent due to their steep SI (Condon et al. 1993; Condon, Helou & Jarrett 2002; Kantharia et al. 2005). Also for the bridge to be bright in synchrotron emission, either in situ star formation is necessary or the tidally disrupted bridge material should have undergone a recent phase of star formation, to give rise to the synchrotron emitting particles. One of the early systems with a radio continuum bridge was Ho 124 (van der Hulst & Hummel 1985). Since then, several other interacting galaxies have been detected with radio bridges such as the Taffy galaxies (Condon et al. 1993). Different processes have been suggested to explain the radio continuum bridges. Condon et al. (1993) have suggested that the bridge magnetic fields and relativistic particles have been stripped from the interpenetrating discs during a nearly head-on collision in the Taffy galaxies. For Ho 124, Kantharia et al. (2005) have suggested that the bridge is likely to be of tidal origin with no evidence of significant star formation in the bridge. In the case of Arp86, both the Hα (Marcelin et al. 1987) and MIR (Smith et al. 2007) images show evidence of star formation in the bridge region. This suggests that the radio continuum bridge could have a significant contribution from star formation between the two galaxies. As mentioned earlier, the SFR in the bridge is $0.6\,M_{\odot}\,{\rm yr}^{-1}$. Deeper images at the other frequencies are required to estimate the spectral index of the bridge.

In the highest resolution map ($7 \times 3\,{\rm arcsec}^2$) at 1394 MHz, the core of NGC 7753 is a resolved source. The spectral index estimated using the 16 arcsec images, which is the resolution of the 240-MHz image, is ∼0.7. The detection of a radio source at the centre of the galaxy is consistent with the identification of a LINER nucleus, a

mildly active galaxy. Although the spectral index is steep, unlike the cores of powerful radio galaxies and quasars, steep SI have been seen in the cores of several mildly active galaxies such as the Seyfert galaxies (Kukula et al. 1993; Thean et al. 2000). This is possibly due to the contamination of the flat-spectrum nucleus by more extended emission.

5 CONCLUSIONS

We present the results of the GMRT observations of the interacting system Arp86 in both neutral atomic hydrogen, H I, and in radio continuum at 240, 606 and 1394 MHz. H I maps of the system reveal disturbed morphology with extended tidal arms and debris suggesting an M51-like interaction. The star-forming regions in the system seem to correlate well with regions of high H I column density. We detect a possible TDG candidate in the system. The tidal bridge is also detected in radio continuum emission. The system is undergoing intense star formation and this probably reflects in an unusually flat SI for the disc emission from NGC 7753 between 606 and 1394 MHz. However, this flattening needs to be confirmed with higher frequency observations.

ACKNOWLEDGMENTS

We thank the reviewer for his/her useful comments and suggestions. We thank the staff of the GMRT who have made these observations possible. The GMRT is operated by the National Centre for Radio Astrophysics of the Tata Institute of Fundamental Research. This research has made use of the NASA/IPAC Extragalactic Data base (NED) which is operated by the Jet Propulsion Laboratory, California Institute of Technology, under contract with the National Aeronautics and Space Administration. CS would like to thank Jayaram Chengalur for some very useful discussions.

REFERENCES

Amram P., Mendes de Oliveira C., Plana H., Balkowski C., Bolte M., 2002, Ap&SS, 281, 397
Baars J. W. M., Genzel R., Pauliny-Toth I. I. K., Witzel A., 1977, A&A, 61, 99
Bell E. F., de Jong R. S., 2001, ApJ, 550, 212
Biermann P., Clarke J. N., Fricke K. J., 1979, A&A, 75, 19
Bruns C. et al., 2005, A&A, 432, 45
Calzetti D. et al., 2005, ApJ, 633, 871
Collison P. M., Saikia D. J., Pedlar A., Axon D. J., Unger S. W., 1994, MNRAS, 268, 203
Condon J. J., Yin Q. F., 1990, ApJ, 357, 97
Condon J. J., Helou G., Sanders D. B., Soifer B. T., 1993, AJ, 105, 1730
Condon J. J., Helou G., Jarrett T. H., 2002, AJ, 123, 1881
de Mello D. F., Smith L. J., Sabbi E., Gallagher J. S., Mountain M., Harbeck D. R., 2008, AJ, 135, 548
Duc P.-A., Brinks E., Springel V., Pichardo B. Weilbacher P., Mirabel I. F., 2000, AJ, 120, 1238
Elmegreen B. G., Kaufman M., Thomasson M., 1993, ApJ, 412, 90
Ferreiro D. L., Pastoriza M. G., Rickes M., 2008, A&A, 481, 645
Franco-Balderas A., Hernández-Toledo H. M., Dultzin-Hacyan D., García-Ruiz G., 2003, A&A, 406, 415
Harris J., 2007, ApJ, 658, 345
Hibbard J. E. et al., 2005, ApJ, 619, 87
Hota A., Saikia D. J., 2005, MNRAS, 356, 998
Howard S., Byrd Gene G., 1990, AJ, 99, 1798
Huang Z. P., Thuan T. X., Chevalier R. A., Condon J. J., Yin Q. F., 1994, ApJ, 424, 114.
Hummel E., 1991, A&A, 251, 442
Huchtmeier W. K., Richter O. G., 1989, A General Catalog of H I Observations of Galaxies, Springer-Verlag, New York
Irwin Judith A., 1994, ApJ, 429, 618
Kantharia N. G., Ananthakrishnan S., Nityananda R., Hota A., 2005, A&A, 435, 483
Karachentsev I. D., Karachentseva V. E., Boerngen F., 1985, MNRAS, 217, 731.
Keel W. C., Kennicutt R. C., Jr, Hummel E., van der Hulst J. M., 1985, AJ, 90, 708
Kennicutt Robert C. Jr, 1989, ApJ, 344, 685
Kukula M. J., Ghosh T., Pedlar A., Schilizzi R. T., Miley G. K., de Bruyn A. G., Saikia D. J., 1993, MNRAS, 264, 893
Larson R. B., Tinsley B. M., 1978, ApJ, 219, 46.
Laurikainen E., Salo H., Aparicio A., 1993, ApJ, 410, 574
Lin L. et al., 2007, ApJ, 660, 51
Marcelin M., Lecoarer E., Boulesteix J., Georgelin Y., Monnet G., 1987, A&A, 179, 101
Maybhate A., Masiero J., Hibbard J. E., Charlton J. C., Palma C., Knierman K. A., English J., 2007, MNRAS, 381, 59
Mihos J. C., Hernquist L., 1994, ApJ, 431, L9
Muller E., Staveley-Smith L., Zealey W., 2004, in Duc P. A., Braine J., Brinks E., eds, IAU Symp. 217, Recycling Intergalactic and Interstellar Matter. Astron. Soc. Pac., San Francisco, p. 506
Mundell C. G., James P. A., Loiseau N., Schinnerer E., Forbes D. A., 2004, ApJ, 614, 648
Neff S. G. et al., 2005, ApJ, 619, 91
Nilson P., 1973, Uppsala General Catalogue of Galaxies. Uppsala Astron. Obs. Ann. 6
Noreau L., Kronberg P. P., 1987, AJ, 93, 1045
Overzier R. A. et al., 2008, ApJ, 677, 37
Prochaska J. X., 2003, ApJ, 582, 49
Rots A. H., Bosma A., van der Hulst J. M., Athanassoula E., Crane P. C., 1990, AJ, 100, 387
Ryan-Weber E. V. et al., 2004, AJ, 127, 1431
Saikia D. J., Phookun B., Pedlar A., Kohno K., 2002, A&A, 383, 98
Salo H., Laurikainen E., 1993, ApJ, 410, 586
Sanders D. B., Scoville N. Z., Young J. S., Soifer B. T., Schloerb F. P., Rice W. L., Danielson G. E., 1986, ApJ, 305L, 45
Skillman E. D., 1987, in Lonsdale C. J., ed., Proc. of Conf. California Institute of Technology, Pasadena, CA, June 16–19, 1986. Star Formation in Galaxies. NASA, Washington, D.C., p. 263
Smith B. J., Struck C., Hancock M., Appleton P. N., Charmandaris V., Reach W. T., 2007, AJ, 133, 791
Thean A., Pedlar A., Kukula M. J., Baum S. A., O'Dea C. P., 2000, MNRAS, 314, 573
Toomre A., 1964, ApJ, 139, 1217
Ulvestad J. S., Antonucci R. R. J., 1997, ApJ, 488, 621
van der Hulst J. M., Hummel E., 1985, A&A, 150, 7
Woods D. F., Geller M. J., 2007, AJ, 134, 527
Worthey G., 1994, ApJS, 95, 107
Yun M. S., Reddy N. A., Condon J. J., 2001, ApJ, 554, 803

This paper has been typeset from a TEX/LATEX file prepared by the author.